Available online at www.sciencedirect.com
ScienceDirect
Trans. Nonferrous Met. Soc. China 32(2022) 2266−2275
Transactions of Nonferrous Metals Society of China
www.tnmsc.cn

TiC strengthened CoCrNi medium entropy alloy: Dissolution and precipitation of TiC and its effect on microstructure and performance

Yong-gang TONG[1], Yan-lin CAI[1], Yong-le HU[1], Hong-feng HUANG[2], Xian-cheng ZHANG[3], Hao ZHANG[1]

1. College of Automobile and Mechanical Engineering,
Changsha University of Science and Technology, Changsha 410114, China;
2. Key Laboratory of New Processing Technology for Nonferrous Metal & Materials, Ministry of Education,
Guilin University of Technology, Guilin 541004, China;
3. School of Mechanical and Power Engineering,
East China University of Science and Technology, Shanghai 200237, China

Received 14 July 2021; accepted 28 December 2021

Abstract: In order to improve the strength and corrosion resistance of CoCrNi medium entropy alloy, TiC strengthened CoCrNi medium entropy alloy (CoCrNi/$(\mathrm{TiC})_x$ (x=0.1, 0.2, 0.4)) was designed by addition of different amounts of TiC. The effects of TiC content on the microstructure, mechanical properties, and corrosion resistance of the alloy were investigated. It was found that the precipitation morphologies of TiC changed from lamellar eutectic to needle structure with the increase of TiC content, and finally formed mixed needled and bulk TiC particles. TiC appears as a dissolution−precipitation phenomenon in the CoCrNi alloy, which is important for the mechanical properties and corrosion resistance of the CoCrNi/$(\mathrm{TiC})_x$ alloy. The strength of alloy was enhanced obviously after the addition of TiC. The compressive yield strength of CoCrNi/$(\mathrm{TiC})_{0.4}$ alloy reached 746 MPa, much larger than that of the CoCrNi medium entropy alloy, 108 MPa. Additionally, the addition of TiC was found to improve the corrosion resistance of CoCrNi medium entropy alloy in the salt solution.

Key words: medium entropy alloy; TiC; corrosion resistance; microstructure; mechanical properties

1 Introduction

Medium entropy alloys are a class of new structure materials with superior properties. Especially, the equiatomic CoCrNi medium entropy alloy has attracted much attention due to its excellent ductility, work hardening, and corrosion resistance [1,2]. In addition, the strength and ductility of CoCrNi medium entropy alloy at low-temperature are improved simultaneously. The tensile strength reached 1300 MPa and the tensile strain increased to 45%. It is an excellent low-temperature structural material with great application potential [3]. Nevertheless, the yield strength of the as-cast CoCrNi medium entropy alloy at room temperature is less than 400 MPa, which limits its extensive application as engineering materials. It is in great demand to improve the room temperature strength in order to promote its industrial applications.

Currently, some investigations have shown that introduction of ceramic particles into the single-phase matrix of medium entropy alloy is an effective method to improve the mechanical properties [4−10]. For example, 5% $\mathrm{Al_2O_3}$ and 5% SiC ceramic particles were added in CoCrFeMnNi high entropy alloy (HEA), respectively, and the

---

Corresponding author: Yong-gang TONG, Tel: +86-18175192496, E-mail: tongyonggang_csust@163.com;
Xian-cheng ZHANG, E-mail: xczhang@ecust.edu.cn

DOI: 10.1016/S1003-6326(22)65946-6

compressive yield strengths of alloys were increased to 1480 and 1600 MPa, respectively [11]. TiC is often used as a reinforcing agent because of its high hardness, high melting point, good wettability, and chemical stability [12−18]. WANG et al [19] prepared TiC reinforced $Fe_{40}Mn_{40}Cr_{10}Co_{10}$ medium entropy alloy with volume fraction of 10% by ball milling combined with spark plasma sintering (SPS). The results show that the compressive strength of the alloy increased from 1571 to 2174 MPa and the hardness increased from HV 320 to HV 872 by adding 10% TiC particles. It is indicated that the introduction of TiC ceramic particles can effectively improve the mechanical properties of medium entropy alloy. In spite of that, it should be noted that the morphologies and distribution of ceramic reinforcement in the alloys, and the dissolution and precipitation process of ceramic particles have a great influence on the microstructure and mechanical properties of the alloys. For example, the microstructure and properties greatly depend on the dissolution and precipitation of WC in cobalt for the WC/Co ceramet [20]. However, up till now, few investigations about the dissolution and precipitation of the TiC ceramic particles in the medium entropy alloy were reported. The behavior of dissolution and precipitation of TiC in this kind of alloys with multi-components is still not clear.

In this work, TiC was selected as the reinforcing agent and TiC strengthened CoCrNi medium entropy alloy, $CoCrNi/(TiC)_x$, was prepared with the different amounts of TiC. The dissolution and precipitation process of TiC in CoCrNi medium entropy alloy and its influence mechanism on microstructure, mechanical properties, and corrosion resistance were studied.

2 Experimental

$CoCrNi/(TiC)_x$ (x=0, 0.1, 0.2, 0.4, and x is the molar ratio) alloys were designed by adding non-equal mole ratio TiC into the CoCrNi medium entropy alloy. The nominal composition of the alloys is listed in Table 1. The raw materials were small pieces of Co, Cr, and Ni with purity of 99.5%, and the added TiC powder with purity of 99.5%. The alloys were prepared by conventional vacuum non-consumptive arc melting method. Argon charging was started when the vacuum in the furnace reached 5×10^{-3} Pa. The melting current was about 400 A. Each alloy was melted five times repeatedly to ensure homogeneous composition. The samples with different molar ratios were marked as T0 (x=0), T1 (x=0.1), T2 (x=0.2), and T4 (x=0.4), respectively.

X-ray diffractometry (XRD, Cu K_α radiation, Rigaku D/Max 2550VB, BRUKER) was used to analyze the phases in the alloy, with a scanning speed of 5 (°)/min and a scanning range of 20°−80°. Scanning electron microscopy (SEM) was used to characterize the microstructure, and energy-dispersive spectrometry (EDS) was used for element composition analysis. HVST−1000Z semi-automatic Vickers hardness tester was used to test the hardness of the alloy (static load: 100 g; holding time: 15 s). Three data points were collected for each sample, and the average value was taken. Samples with the sizes of d5 mm × 8 mm were cut from the ingots, and a CMT5105GL electronic universal tensile testing machine was used to test the compressive mechanical properties at room temperature with a loading rate of 0.5 mm/min (without extensometer). 3.5 wt.% NaCl solution of 25 °C and neutral pH range was used to simulate seawater environment and conduct electrochemical corrosion test. Electrochemical polarization was carried out in a typical three-electrode battery, consisting of a sample as a working electrode, a platinum sheet as a counter electrode, and a saturated calomel electrode as a reference electrode. Before all electrochemical tests, the samples were sealed with epoxy resin, leaving only 1 cm^2 of the metal surface in contact with the electrolyte, and immersed in the solution for 30 min. The electrochemical parameters were controlled by Solartron 1470E analyzer. The potentiodynamic polarization tests were performed at a potential ranging from −0.25 to 1.5 V and a scanning rate of 1 mV/s.

Table 1 Nominal composition of $CoCrNi/(TiC)_x$ (x=0, 0.1, 0.2, 0.4) medium entropy alloy

Alloy No.	Alloying constituent	Molar ratio			
		Co	Cr	Ni	TiC
T0	CoCrNi	1	1	1	0
T1	$CoCrNi/(TiC)_{0.1}$	1	1	1	0.1
T2	$CoCrNi/(TiC)_{0.2}$	1	1	1	0.2
T4	$CoCrNi/(TiC)_{0.4}$	1	1	1	0.4

3 Results and discussion

3.1 XRD analysis

XRD patterns of CoCrNi/$(TiC)_x$ (x=0, 0.1, 0.2, 0.4) medium entropy alloys are shown in Fig. 1. The results show that a single solid solution of FCC was formed in CoCrNi alloy, which is consistent with the previous research [21]. With the addition of TiC, the Sample T1 is still FCC phase, and the diffraction peaks shift to the left. No obvious TiC phase diffraction peaks were found. When x=0.2, TiC diffraction peaks appear in Sample T2. Here, the alloy structure begins to transform from single-phase FCC to FCC + TiC dual phases. With the further increase of TiC content, TiC in the Sample T4 increases significantly, while the diffraction peak intensity of the FCC phase decreases obviously.

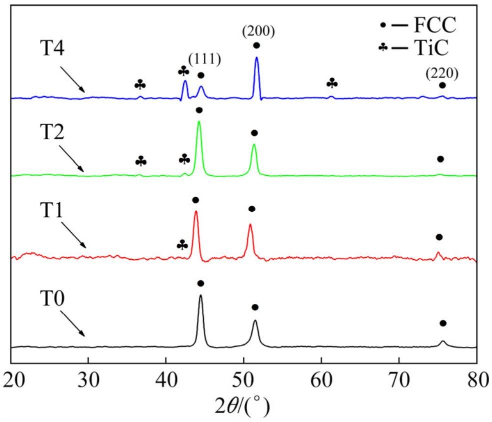

Fig. 1 XRD patterns of CoCrNi/$(TiC)_x$ (x=0, 0.1, 0.2, 0.4) medium entropy alloys

3.2 Microstructure

The morphology of the original TiC powder for the fabrication of the alloys is shown in Figs. 2(g) and (h). It can be seen that the original TiC is bulk particles with an average size smaller than 5 μm. Microstructure of CoCrNi/$(TiC)_x$ (x=0.1, 0.2, 0.4) medium entropy alloy is shown in Figs. 2(a)−(e). It can be seen from Figs. 2(a) and (b) that TiC precipitated as lamellar eutectic in Sample T1. With the increase of TiC content, lamellar eutectic precipitates disappeared in Sample T2 (Figs. 2(c) and (d)), and lots of needled TiC precipitated along the grain boundary. A small amount of TiC particles were also found in Sample T2 in some partial areas. The width of needled TiC is less than 1 μm and the length varies from a few microns to a dozen microns. With further increasing TiC content, it is found that the precipitates are mainly needled and bulk TiC ceramic particles in Sample T4 (Fig. 2(e)), and the needled structure was significantly reduced.

Based on the above characterization, it is obvious that the TiC morphologies in CoCrNi/$(TiC)_x$ alloy present a gradual precipitation phenomenon with the increase of the TiC addition. The precipitated morphologies change from the initial lamellar eutectic to needled shape and finally evolve into bulk particles. Compared with the original TiC morphology, the precipitation morphologies of TiC in the alloy are quite different from the original TiC morphology. This indicates that TiC dissolves and reprecipitates in CoCrNi alloy. In order to further identify the composition of the phases, EDS analysis was carried out and the results are shown in Table 2 and Fig. 3. When TiC content is low, the solubility of TiC into the alloy is high and TiC precipitates in the form of lamellar eutectic. It can be seen from EDS results in Table 2 and Fig. 3 that there are a small amount of Ti and C elements in the CoCrNi matrix, which proves that the CoCrNi alloy has a certain solubility for TiC. With the increase of TiC content, lamellar eutectic disappeared and needled TiC appeared in Sample T2, indicating that TiC content exceeded the eutectic point. When the TiC content further increases, the volume fraction of block TiC ceramic phase increases, and needled TiC decreases obviously in Sample T4. The needled TiC preferentially nucleates and grows into block TiC particles with sizes ranging from several microns to more than ten microns. If TiC content continues to increase, the block TiC ceramic phase will be expected to grow. In order to confirm this, the equimolar ratio of CoCrNi/TiC alloy was prepared by adding higher content of TiC into CoCrNi alloy, and its microstructure is shown in Fig. 2(f). It was found that when the TiC content reached 25%, the precipitated block TiC phase was more densely distributed in the CoCrNi alloy. The bulk TiC grows obviously and its size increases to about tens of microns, accompanied by the decrease of needled TiC phase. In addition to the dissolution and reprecipitation of TiC, EDS results also showed some Cr segregation in partial areas in Samples T2 and T4. This is not a common phenomenon, so we did not further discuss and mention it.

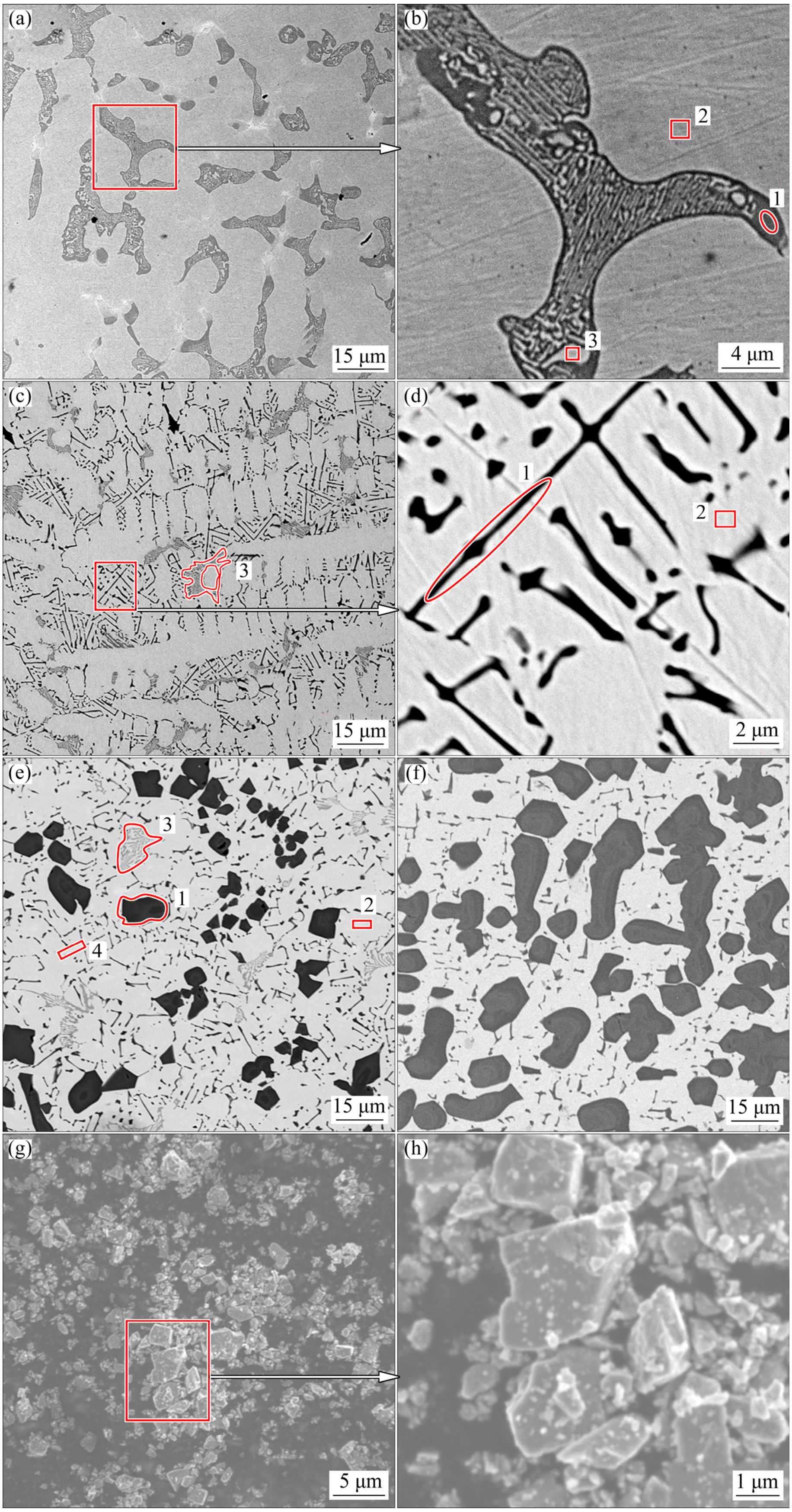

Fig. 2 SEM images of CoCrNi/$(TiC)_x$ (x=0.1, 0.2, 0.4) medium entropy alloys and TiC powder: (a, b) CoCrNi/$(TiC)_{0.1}$; (c, d) CoCrNi/$(TiC)_{0.2}$; (e) CoCrNi/$(TiC)_{0.4}$; (f) CoCrNi/TiC; (g, h) TiC powder

Table 2 EDS analysis results of typical micro zones in Fig. 2 (at.%)

Position	Co	Cr	Ni	Ti	C
Entire area of Fig. 2(a)	28.52	24.47	27.71	9.88	9.22
Fig. 2(b)-1	19.41	4.75	24.70	16.76	34.39
Fig. 2(b)-2	18.94	19.45	16.26	2.97	42.37
Fig. 2(b)-3	18.37	17.43	17.97	5.98	40.25
Entire area of Fig. 2(c)	27.68	26.57	27.04	4.93	13.77
Fig. 2(c)-3	10.73	37.96	9.00	1.38	40.94
Entire area of Fig. 2(d)	27.68	26.57	27.04	13.77	4.93
Fig. 2(d)-1	6.28	12.57	5.81	24.96	50.38
Fig. 2(d)-2	24.06	19.51	23.44	1.87	31.12
Entire area of Fig. 2(e)	22.47	23.77	21.97	10.30	21.49
Fig. 2(e)-1	−	−	−	56.12	43.88
Fig. 2(e)-2	28.44	23.98	26.75	2.10	18.73
Fig. 2(e)-3	4.08	60.01	−	1.28	34.63
Fig. 2(e)-4	11.34	17.13	11.05	24.49	35.99

Based on the above analysis and verification, the dissolution and precipitation process of TiC in CoCrNi alloy is summarized, and the evolution diagram is shown in Fig. 4. When the TiC content is low and not enough to precipitate, the TiC particles are dissolved in the CoCrNi alloy (Fig. 4(I)). With the increase of TiC content, the excess TiC particles start to accumulate and precipitate out of the matrix, forming a two-phase structure with the coexistence of FCC matrix and eutectic TiC (Fig. 4(II)). When the TiC content continues to increase, the eutectic structure disappears and is replaced by the dense precipitation of needle-like TiC at the grain boundaries (Fig. 4(III)). If the TiC content continues to increase, a large amount of TiC will form bulk TiC ceramic particles, which will eventually form the structure in the CoCrNi alloy as shown in Fig. 4(IV). This is dominated by the precipitation of needle-like and bulk TiC ceramic particles. Finally, if the TiC continues to be added, the tissue structure remains basically unchanged, and the size and volume fraction of bulk TiC precipitates will further increase, accompanied by a gradual decrease in the volume fraction of needle-like TiC.

3.3 Mechanical properties

To investigate the addition of TiC on mechanical properties of the CoCrNi/(TiC)$_x$ alloys, Vickers hardness and compression properties of the alloys were measured and listed in Table 3. Figure 5 shows the compression engineering stress−strain curves of Samples T0, T1, T2, and T4 at room temperature. Compared with CoCrNi alloy, the compressive yield strength of CoCrNi/(TiC)$_x$ is obviously improved from 188 to 746 MPa. In addition, the compressive strength of Samples T2 and T4 increased to 1430 and 1850 MPa, and the fracture strains were still 36% and 28%. Addition of TiC significantly improves the strength of CoCrNi alloy. As shown in Fig. 5 and Table 3, different shaped TiC precipitates from the CoCrNi/(TiC)$_x$ alloys and some Ti and C atoms dissolve into the alloy's matrix. Thus, the strength enhancement of alloy can be mainly attributed to the solid solution strengthening and the second phase strengthening of TiC. Similar to the mechanical properties, the microhardness also increases with the addition of TiC as shown in Fig. 6. The microhardness of Samples T1, T2 and T4 was increased to HV 324, HV 355 and HV 503, respectively. Compared with CoCrNi alloy, the hardness of Sample T4 increased by 160%. The increase of Vickers hardness is also attributed to the precipitation and strengthening of TiC for the alloys.

The fracture surface morphologies of CoCrNi/(TiC)$_x$ (x=0.2, 0.4) after compressive tests are shown in Fig. 7. The Samples T0 and T1 were pressed into the cake without fracture, indicating

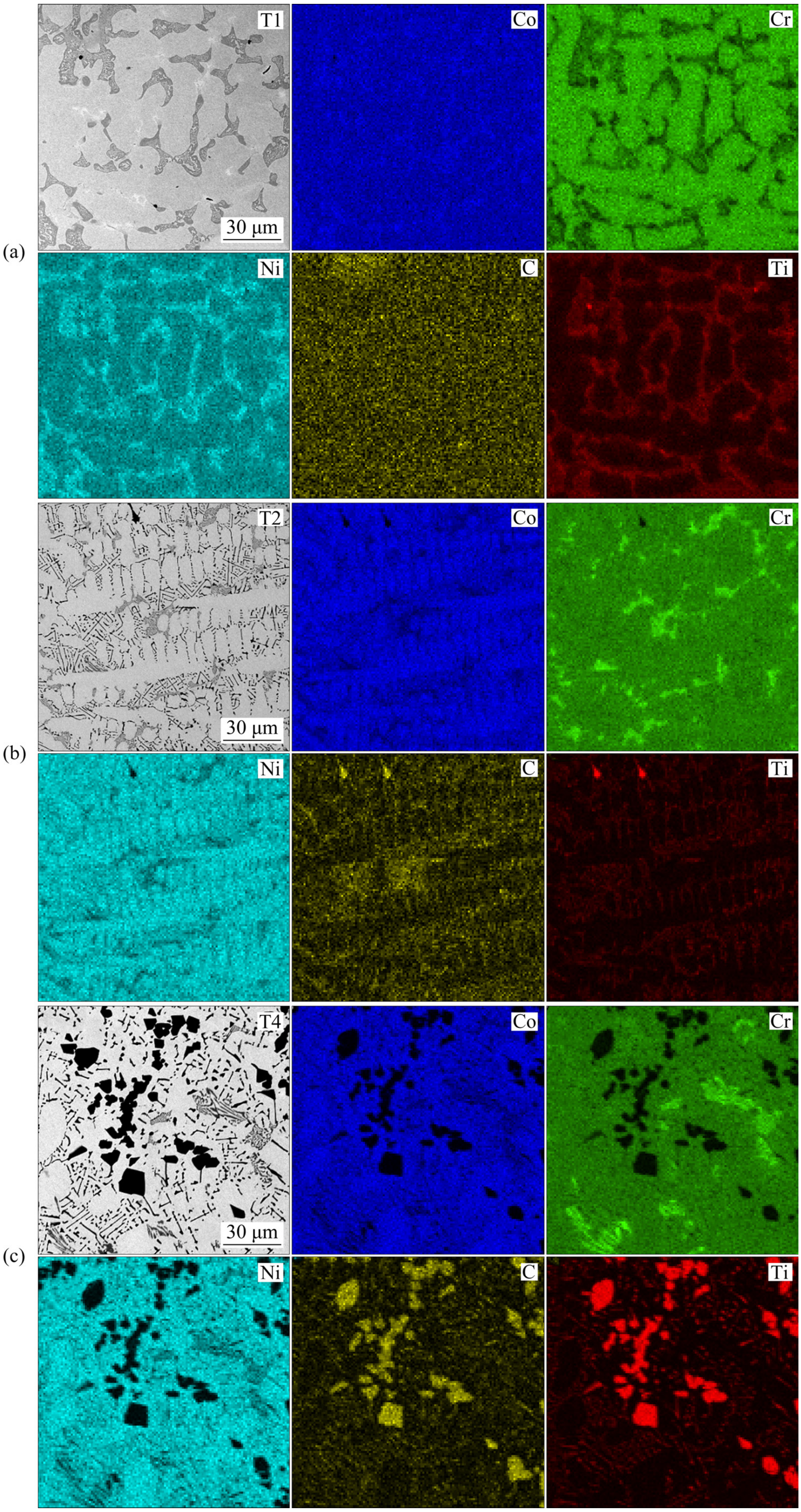

Fig. 3 Elemental maps of selected regime in CoCrNi/$(TiC)_x$ (x=0.1, 0.2, 0.4) medium entropy alloys: (a) T1; (b) T2; (c) T4

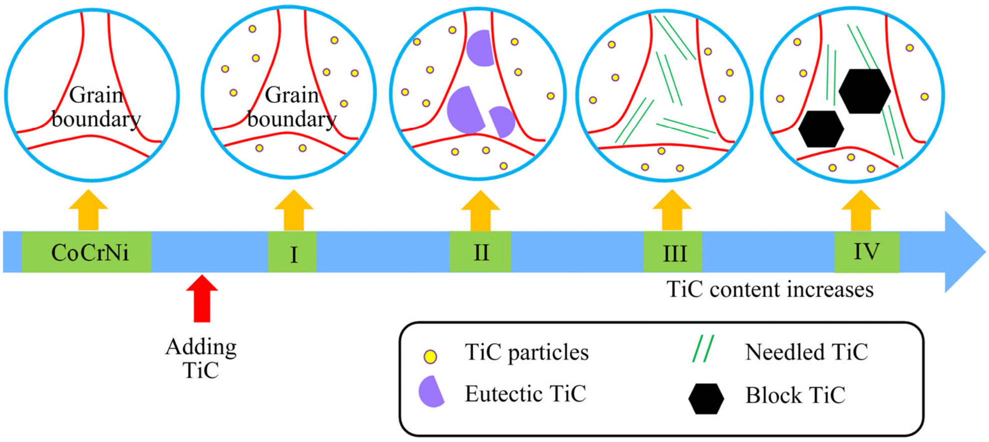

Fig. 4 Diagram of microstructure evolution with increasing TiC content in CoCrNi alloy

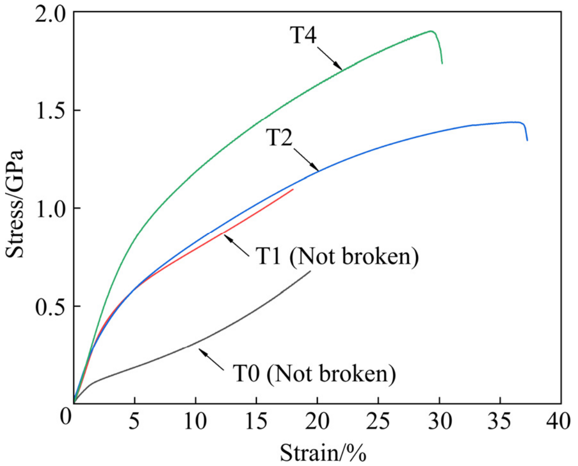

Fig. 5 Typical engineering stress−strain curves of CoCrNi/$(TiC)_x$ (x=0, 0.1, 0.2, 0.4) medium entropy alloys

Table 3 Mechanical properties of CoCrNi/$(TiC)_x$ (x=0, 0.1, 0.2, 0.4) medium entropy alloys

Alloy No.	Compressive yield strength/MPa	Compressive strength/MPa	Fracture strain/%
T0	108	−	−
T1	413	−	−
T2	500	1430	36
T4	746	1900	29

that CoCrNi alloy and Sample T1 have excellent plasticity. A small number of dimples were found in Sample T2 (Fig. 7(a_1)). These dense dimples are the main contributors to the plasticity of Sample T2. With the increase of TiC content, obvious dissociation steps and tongue-like patterns can be observed in Figs. 7(b_1) and (b_2). It shows that the precipitation of block TiC makes the fracture mode of Sample T4 change from ductile fracture to brittle fracture.

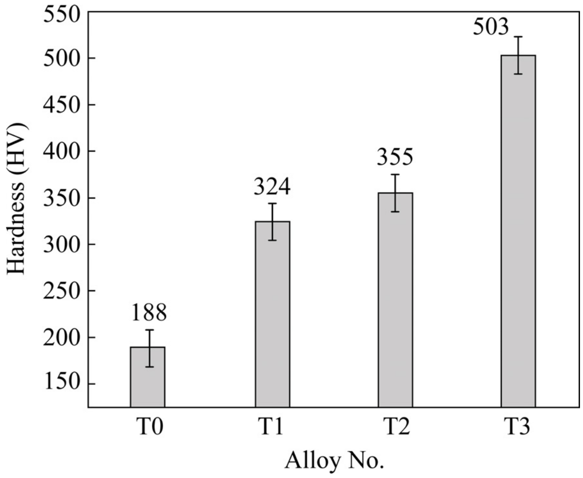

Fig. 6 Variation of Vickers hardness of CoCrNi/$(TiC)_x$ (x=0, 0.1, 0.2, 0.4) medium entropy alloys

3.4 Corrosion performance

Figure 8 shows potentiodynamic polarization curves of CoCrNi/$(TiC)_x$ (x=0, 0.1, 0.2, 0.4) alloys in 3.5 wt.% NaCl solution. It can be seen from Fig. 8 that all polarization curves do not show activation−passivation region. After adding TiC, the activation region of the anode shifted to the left obviously. It suggests that the corrosion current (J_{corr}) decreases. According to the polarization curve, the increase of corrosion resistance is mainly due to the decrease of corrosion current density. Combined with Table 4, the corrosion current density of the alloys decreased by an order of magnitude after adding TiC, and gradually decreased with the increase of TiC content. Compared with CoCrNi alloy, the corrosion current density of Sample T4 is reduced by nearly 80%, indicating that Sample T4 has the best corrosion performance.

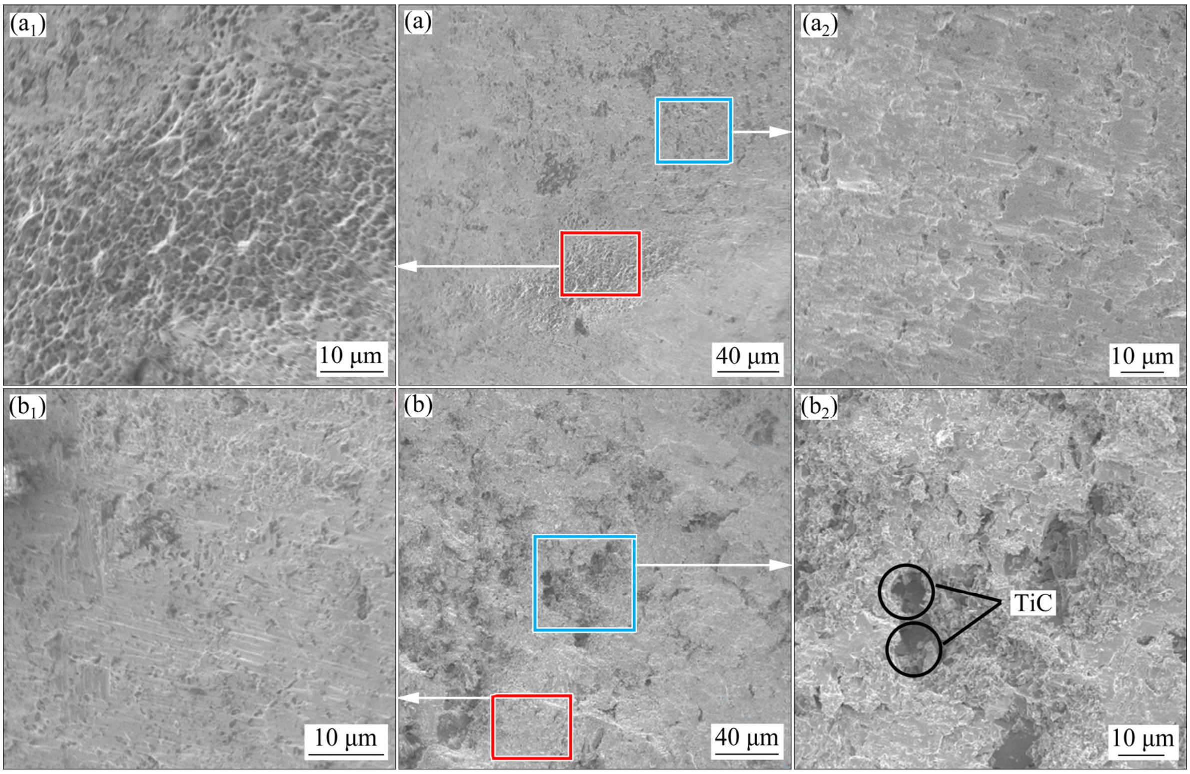

Fig. 7 Fracture surfaces of CoCrNi/$(TiC)_x$ (x=0.2, 0.4) medium entropy alloy: (a, a_1, a_2) CoCrNi/$(TiC)_{0.2}$; (b, b_1, b_2) CoCrNi/$(TiC)_{0.4}$

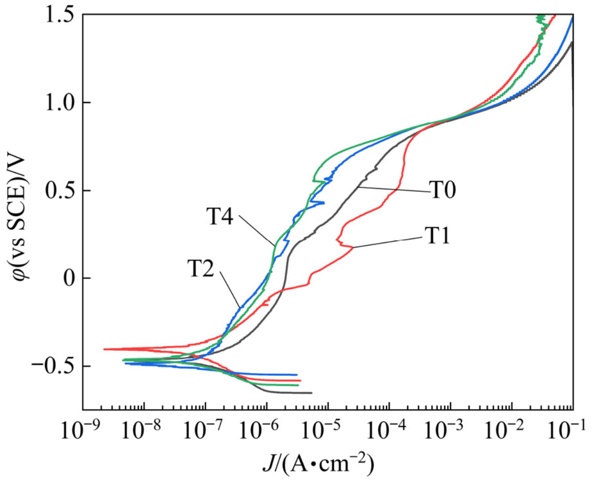

Fig. 8 Polarization curves of CoCrNi/$(TiC)_x$ (x=0, 0.1, 0.2, 0.4) medium entropy alloys

Table 4 Parameters of potentiodynamic polarization curves of CoCrNi/$(TiC)_x$ (x=0, 0.1, 0.2, 0.4) medium entropy alloys

Alloy No.	φ_{corr}(vs SCE)/V	$J_{corr}/(A\cdot cm^{-2})$
T0	−0.46694	1.63×10^{-7}
T1	−0.40005	6.51×10^{-8}
T2	−0.48838	3.92×10^{-8}
T4	−0.56905	3.46×10^{-8}

4 Conclusions

(1) TiC was dissolved and precipitated in CoCrNi alloy. TiC was dissolved in CoCrNi alloy when TiC content was low. With the increase of TiC content, the precipitation morphology of TiC changed from lamellar eutectic to needle structure and finally formed needle and bulk mixed structure.

(2) The strength and hardness of CoCrNi/$(TiC)_x$ alloy increase with TiC content addition due to the solution strengthening and the second phase strengthening. The compressive strength of CoCrNi/$(TiC)_{0.4}$ alloy was increased to 1850 MPa, and the fracture strain was 28%. The hardness of the alloy was increased from HV 188 to HV 503.

(3) With the increase of TiC content, the corrosion current density of CoCrNi/$(TiC)_x$ alloy decreased gradually in 3.5 wt.% NaCl solution, and the corrosion resistance of CoCrNi/$(TiC)_x$ medium entropy alloys increased gradually.

Acknowledgments

This work was sponsored by the National Key R&D Program of China (No. 2018YFC1902401), the National Natural Science Foundation of China

(No. 52005053), and Open Fund of Key Laboratory of New Processing Technology for Nonferrous Metal & Materials Ministry of Education, China (No. 20KF-24).

References

[1] SLONE C E, MIAO J, GEORGE E P, MILLS M J. Achieving ultra-high strength and ductility in equiatomic CrCoNi with partially recrystallized microstructures [J]. Acta Materialia, 2019, 165: 496−507.

[2] MA Yan, YUAN Fu-ping, YANG Mu-xin, JIANG Ping, MA E, WU Xiao-le. Dynamic shear deformation of a CrCoNi medium-entropy alloy with heterogeneous grain structures [J]. Acta Materialia, 2018, 148: 407−418.

[3] GLUDOVATZ B, HOHENWARTER A, THURSTON K V S, BEI H B, WU Z G, GEORGE E P, RITCHIE R O. Exceptional damage-tolerance of a medium-entropy alloy CrCoNi at cryogenic temperatures [J]. Nature Communications, 2016, 7: 10602.

[4] KHORSHID M T, JAHROMI S A J, MOSHKSAR M M. Mechanical properties of tri-modal Al matrix composites reinforced by nano- and submicron-sized Al_2O_3 particulates developed by wet attrition milling and hot extrusion [J]. Materials & Design, 2010, 31: 3880−3884.

[5] CASATI R, VEDANI M. Metal matrix composites reinforced by nano-particles—A review [J]. Metals, 2014, 4: 65−83.

[6] CHEN C S, YANG C C, CHAI H Y, YEH J W, CHAU J L H. Novel cermet material of WC/multi-element alloy [J]. International Journal of Refractory Metals and Hard Materials, 2014, 43: 200−204.

[7] ZHU Gang, LIU Ying, YE Jin-wen. Early high-temperature oxidation behavior of Ti(C, N)-based cermets with multi-component AlCoCrFeNi high-entropy alloy binder [J]. International Journal of Refractory Metals and Hard Materials, 2014, 44: 35−41.

[8] ROGAL Ł, KALITA D, LITYNSKA-DOBRZYNSKA L. CoCrFeMnNi high entropy alloy matrix nanocomposite with addition of Al_2O_3 [J]. Intermetallics, 2017, 86: 104−109.

[9] SHEN Q K, KONG X D, CHEN X Z, YAO X K, DEEV V B, PRUSOV E S. Powder plasma arc additive manufactured CoCrFeNi$(SiC)_x$ high-entropy alloys: Microstructure and mechanical properties [J]. Materials Letters, 2021, 282: 128736.

[10] CAI Yang-chuan, ZHU Li-song, CUI Yan, SHAN Meng-die, LI Hui-jun, XIN Yi, HAN Jian. Fracture and wear mechanisms of FeMnCrNiCo+x(TiC) composite high-entropy alloy cladding layers [J]. Applied Surface Science, 2021, 543: 148794.

[11] SHEN Lin, ZHAO Yue, LI Yu-lu, WU Hao, ZHU He-guo, XIE Zong-han. Synergistic strengthening of FeCrNiCo high entropy alloys via micro-TiC and nano-SiC particles [J]. Materials Today Communications, 2021, 26: 101729.

[12] CHENG Jiang-bo, LIU Dan, LIANG Xiu-bing, CHEN Yong-xiong. Evolution of microstructure and mechanical properties of in situ synthesized TiC−TiB_2/CoCrCuFeNi high entropy alloy coatings [J]. Surface and Coatings Technology, 2015, 281: 109−116.

[13] SUN Xiao-dong, ZHU He-guo, LI Jian-liang, HUANG Jie-wen, XIE Zong-han. High entropy alloy FeCoNiCu matrix composites reinforced with in-situ TiC particles and graphite whiskers [J]. Materials Chemistry and Physics, 2018, 220: 449−459.

[14] WANG Hong-wei, QI Ji-qiu, ZOU Chun-ming, ZHU Dong-dong, WEI Zun-jie. High-temperature tensile strengths of in situ synthesized TiC/Ti-alloy composites [J]. Materials Science and Engineering A, 2012, 545: 209−213.

[15] FAN Qi-chao, LI Bang-sheng, ZHANG Yong-hao. The microstructure and properties of (FeCrNiCo)Al_xCu_y high-entropy alloys and their TiC-reinforced composites [J]. Materials Science and Engineering A, 2014, 598: 244−250.

[16] FU Z Z, KOC R. TiNiFeCrCoAl high-entropy alloys as novel metallic binders for TiB_2−TiC based composites [J]. Materials Science and Engineering A, 2018, 735: 302−309.

[17] HE Long, TAN Ye-fa, TAN Hua, ZHOU Chun-hua, GAO Li. Tribological properties of nanostructured Al_2O_3−40%TiO_2 multiphase ceramic particles reinforced Ni-based alloy composite coatings [J]. Transactions of Nonferrous Metals Society of China, 2013, 23: 2618−2627.

[18] CHEN Jing-bo, HUANG Li-mei, LUO Lai-ma, ZAN Xiang, WU Yu-cheng. Influence of TiC content on microstructure and properties of W−30Cu/TiC composites [J]. Rare Metal Materials and Engineering, 2018, 47(2): 447−451.

[19] WANG Jian-ying, FANG Jing-hua, YANG Hai-lin, LIU Zhi-lin, LI Rui-di, JI Shou-xun, WANG Yun, RUAN Jian-ming. Mechanical properties and wear resistance of medium entropy $Fe_{40}Mn_{40}Cr_{10}Co_{10}$/TiC composites [J]. Transactions of Nonferrous Metals Society of China, 2019, 29: 1484−1494.

[20] KAMBAKAS K, TSAKIROPOULOS P. Solidification of high-Cr white cast iron–WC particle reinforced composites [J]. Materials Science and Engineering A, 2005, 413/414: 538−544.

[21] WANG Jian-ying, YANG Hai-lin, RUAN Jian-ming, WANG Yun, JI Shou-xun. Microstructure and properties of CoCrNi medium-entropy alloy produced by gas atomization and spark plasma sintering [J]. Journal of Materials Research, 2019, 34: 2126−2136.

TiC 强化 CoCrNi 中熵合金：
TiC 溶解析出及其对显微组织和性能的影响

仝永刚 1，蔡炎林 1，胡永乐 1，黄宏锋 2，张显程 3，张 浩 1

1. 长沙理工大学 汽车与机械工程学院，长沙 410114；
2. 桂林理工大学 有色金属及材料加工新技术教育部重点实验室，桂林 541004；
3. 华东理工大学 机械与动力工程学院，上海 200237

摘 要：为了提高 CoCrNi 中熵合金的强度和耐腐蚀性能，通过添加不同含量 TiC 设计 TiC 强化 CoCrNi 中熵合金 (CoCrNi/(TiC)$_x$ (x=0.1, 0.2, 0.4))。研究 TiC 含量对合金的显微组织、力学性能和耐腐蚀性的影响。研究发现，随着 TiC 含量的增加，TiC 的析出形态从片状共晶转变为针状结构，最后形成针状与块状 TiC 混合颗粒。TiC 在 CoCrNi 合金中出现溶解−析出现象，这对 CoCrNi/(TiC)$_x$ 合金的力学性能和耐腐蚀性能具有重要意义。加入 TiC 后，合金的强度明显提高。CoCrNi/(TiC)$_{0.4}$ 合金的抗压屈服强度达到 746 MPa，远高于 CoCrNi 中熵合金的 108 MPa。此外，TiC 的加入还能提高 CoCrNi 中熵合金在盐溶液中的耐腐蚀性。

关键词：中熵合金；TiC；耐腐蚀性；显微组织；力学性能

(Edited by Xiang-qun LI)